Calcium and Magnesium Binding to Human Centrin 3 and Interaction with Target Peptides†

Jos A. Cox,‡ Fabiana Tirone,‡ Isabelle Durussel,‡ Claudia Firanescu,§ Yves Blouquit,§ Patricia Duchambon,§ and Constantin T. Craescu*,§

Department of Biochemistry, University of Geneva, Geneva 4, Switzerland, and INSERM/Institut Curie, Centre Universitaire Paris-Sud, Bâtiment 112, 91405 Orsay Cedex, France

Received August 9, 2004; Revised Manuscript Received November 2, 2004

ABSTRACT: There are four isoforms of centrin in mammals, with variable sequence, tissue expression, and functional properties. We have recently characterized a number of structural, ion, and target binding properties of human centrin isoform HsCen2. This paper reports a similar characterization of HsCen3, overexpressed in *Escherichia coli* and purified by phase-reversed chromatography. Equilibrium and dynamic binding studies revealed that HsCen3 has one mixed Ca^{2+}/Mg^{2+} binding site of high affinity ($K_d = 3$ and 10 μM for Ca^{2+} and Mg^{2+}, respectively) and two Ca^{2+}-specific sites of low affinity ($K_d = 140$ μM). The metal-free protein is fragmented by an unidentified protease into a polypeptide segment of 11 kDa, which was purified by HPLC, and identified by mass spectrometry as the segment of residues 21−112. Similarly, controlled trypsinolysis on Ca^{2+}-bound HsCen3 yielded a mixture of segments of residues 1−124 and 1−125. The Ca^{2+}/Mg^{2+} site could be assigned to this segment and thus resides in the N-terminal half of HsCen3. Temperature denaturation experiments, circular dichroism, and utilization of fluorescence hydrophobic probes allowed us to propose that the metal-free protein has molten globule characteristics and that the dication-bound forms are compact with a polar surface for the Mg^{2+} form and a hydrophobic exposed surface for the Ca^{2+} form. Thus, HsCen3 could be classified as a Ca^{2+} sensor protein. In addition, it is able to bind strongly to a model target peptide (melittin), as well as to peptides derived from the protein XPC and Kar1p, with a moderate Ca^{2+} dependence.

In higher eukaryotes, the number, direction, and polarity of microtubules are organized by the centrosome, which, in interphase, is composed of two centrioles surrounded by a pericentriolar material containing ∼100 proteins. Before mitosis, this complex structure duplicates and forms the two poles of the mitotic spindle (for a review, see ref *1*). It is now widely accepted that abnormal centrosome duplication and its possible correlation with an altered chromosome integrity may promote a cancer phenotype (*2*−*4*). Calcium and calcium-modulated proteins, including calmodulin and some protein kinases, are required in several key steps of the cell cycle like the G_1−S, G_2−M, and metaphase−anaphase transitions (*5*).

Centrins, members of the EF-hand superfamily, and closely related to calmodulin, are part of the centrosome structure and are essential components of the centriole duplication process (*6*−*8*). The four vertebrate centrin isoforms that have been identified so far can be classified into three phylogenetic groups, each including a murine variant (MmCen1−MmCen4)[1] (*9, 10*). Comparative sequence analysis suggested the existence of two divergent subfamilies: MmCen1, MmCen2, MmCen4, and centrin from *Chlamydomonas* (CrCen) belong to one branch, while MmCen3 and the yeast homologue Cdc31p belong to another branch (*10*). Sequence similarity patterns seem to be poorly correlated to the tissue expression profiles, splicing variability, or cellular localization. The study of specific cell or tissue expression of vertebrate centrins was hampered by the lack of monoclonal antibodies, able to discriminate among the four isoforms. The available results show that while MmCen2 and MmCen3 appear to be ubiquitously expressed, MmCen1 and MmCen4 have a tissue-specific expression profile, being mainly detected in the male germ cells (MmCen1) (*11*) or in brain, lung, kidney, and ovary (MmCen4) (*9*). Fluorescence and electron microscopy revealed that members of the two subfamilies of mammalian centrins may be found in the distal lumen of the centrioles and in the pericentriolar material (*9*, *12*), but larger quantities are present in other cell compartments, like the nucleus or the submembrane space (*12*). The yeast centrin homologue Cdc31p localizes to the half-bridge

† This work was supported by the Institut Curie, the Institut National pour la Santé et la Recherche Médicale, and the Centre National de la Recherche Scientifique. C.F. was the recipient of a FEBS fellowship.

* To whom correspondence should be addressed. Telephone: 33 1 69 86 31 63. Fax: 33 1 69 07 53 27. E-mail: Gil.Craescu@curie.u-psud.fr.

‡ University of Geneva.

§ Centre Universitaire Paris-Sud.

[1] Abbreviations: CaM, calmodulin; CaVP, calcium vector protein; CD, circular dichroism; CrCen, *Chlamydomonas reinhardtii* centrin; CLSP, calmodulin-like skin protein; DSS, disuccinimidyl suberate; HsCen, human centrin; ITC, isothermal titration calorimetry; ME, melittin; MG, molten globule; MmCen1−MmCen4, murine centrin isoforms 1−4, respectively; NER, nucleotide excision repair; NSCP, *Nereis* sarcoplasmic Ca^{2+}-binding protein; PAGE, polyacrylamide gel electrophoresis; SPB, spindle pole body; TnC, troponin C; TNS, 2-*p*-toluidinylnaphthalene-6-sulfonate; XPC, xeroderma pigmentosum group C protein.

10.1021/bi048294e CCC: $30.25
Published on Web 12/31/2004

of the spindle pole body (SPB) that crosses the nuclear envelope (*13*).

The functions of centrins are actually poorly understood. Using RNA interference to reduce the levels of HsCen2 in HeLa cells, Salisbury et al. (*7*) observed a progressive loss of centrioles, due to a complete block of centriole duplication. During subsequent cycles, the cells accumulate several nuclei and finally die. Similar observations were made for the duplication of basal bodies in the green algae (*6*, *14*). Centrins may play an additional role as components of Ca^{2+}-sensitive contractile fibers attached to centrosomes/basal bodies, as in the striated flagellar roots of green algae (*15*, *16*). The precise structural and dynamic basis of centrin function in the motility and contractility phenomena observed in the ciliated cells is currently a matter of speculation.

Like other proteins from the CaM subfamily, centrins seem to act as a Ca^{2+} sensor; i.e., in their Ca^{2+}-loaded form, they interact with specific target proteins to modulate their cellular activity (*17*). HsCen2 and CrCen, which are the two best characterized members, exhibit very different Ca^{2+} binding properties. HsCen2 binds only one Ca^{2+} per molecule with a significant affinity ($K_d = 30\ \mu M$), apparently through EF-hand IV (*18*, *19*). In contrast, CrCen binds four Ca^{2+} ions per monomer at two independent pairs of EF-hands with K_d values of $1-10\ \mu M$ for the N-terminal domain and distinct affinities (micromolar and millimolar) for the C-terminal pairs (*20*).

The first centrin−target interaction was described in the yeast SPB, where Cdc31p can bind to a nuclear membrane protein of the half-bridge, named Kar1p, with a K_d of 60 nM (*21*). The centrin binding site of Kar1p (that has no mammalian homologue) is centered around the fragment of residues $K_{239}-K_{257}$ (*22*). HsCen1 and HsCen2, but not MmCen4, also bind to this peptide with a lower (~10 times) affinity (*9*, *22*). Other potential protein targets in the SPB were recently proposed, including mps3p (*23*) and Sfi1 (*24*), both having homologues in higher-eukaryote centrosomes.

Recently, two potential centrin targets were identified outside the centrosome, i.e., the nuclear protein complex NER (nucleotide excision repair) (*25*) and the nuclear mRNA export machinery (*26*). In the NER process, HsCen2 was found to be associated with the heterodimer formed by the XPC protein (for xeroderma pigmentosum group C) and the hHR23B protein, that was shown to recognize and bind to the damaged DNA, and then recruit other proteins such as transcription factor complex TFIIH (*25*). Using a combined theoretical and experimental approach, we identified a 17-residue XPC fragment (P1-XPC) having a high affinity ($K_d = 4.5$ nM) for HsCen2 (*17*). In the mRNA export complex, a nucleoporin-associated factor called Sac3 also interacts with yeast centrin Cdc31p, and although the precise location of the centrin-binding site has still not been identified, a particular segment ($K_{733}-R_{860}$) in the C-terminal domain is a good candidate (*26*). Transducin, a G-protein from visual signal transduction, was recently proposed as another potential centrin target in mammalian photoreceptor cells (reviewed in ref *10*). HsCen2 is also able to bind a natural peptide mimicking the CaM targets, melittin ($K_d = 100$ nM) (*18*).

To understand the functional significance of the high level of diversity in sequence, tissue expression, cell localization, and biological functions of various human centrin isoforms, a comprehensive molecular characterization of the different polypeptides is required. The aim of this work was to study the molecular properties of HsCen3, including Ca^{2+} binding, Ca^{2+}-induced conformational changes, and interactions with target peptides. Unexpectedly, we located a single high-affinity Ca^{2+}/Mg^{2+} mixed site in the N-terminal half. The apo state of HsCen3, which is a molten globule (MG), adopts a compact state with polar surface upon binding of Mg^{2+}, and a well-structured state with exposed hydrophobic surface upon binding of Ca^{2+}. Like HsCen2, HsCen3 shows a high-affinity interaction with melittin and P1-XPC.

EXPERIMENTAL PROCEDURES

Materials. HsCen3 was cloned into expression vector pET Blue-1 (Novagen). The vector was transferred into *Escherichia coli* Tuner (DE3) pLacI, overexpressed, and purified as previously described for HsCen2 (*18*). Small amounts of impurities were removed by chromatography on DE52 cellulose in Tris-HCl (pH 7.5) with a linear gradient of KCl, all in 90 μM Ca^{2+}. The protein was eluted at 150 mM KCl and was pure as analyzed by SDS−PAGE. The concentrations for HsCen3 and its 11 kDa fragment (see below) were determined spectrophotometrically using an extinction coefficient (ϵ_{278}) of 8250 $M^{-1}\ cm^{-1}$, based on the Trp and Tyr content. ME was purified as described previously (*27*). Its concentration was assessed spectrophotometrically using an ϵ_{280} of 5500 $M^{-1}\ cm^{-1}$. The peptides P1-XPC (corresponding to residues $N_{847}-R_{863}$ of the human XPC protein) and P-Kar1p (corresponding to residues $K_{239}-K_{257}$ of the yeast Kar1p protein) were purchased from BIOFIDAL (Vaulx-en-Velin, France). The purity was greater than 95%, as assessed by high-pressure liquid chromatography analysis.

Mass Spectrometry. The molecular masses of whole HsCen3, its 11 kDa endogenous fragment (see the Results), and the 14 kDa tryptic fragment were determined by MALDI-TOF mass spectrometry. To localize the 11 kDa endogenous fragment in the sequence of HsCen3, its SDS−PAGE protein band was digested *in situ* with trypsin, the extracted peptides were analyzed by MALDI-TOF mass spectrometry, and the obtained molecular weights were compared to those of the known trypsin peptides in HsCen3.

Metal Removal and Cation Binding. HsCen3 or its 11 kDa fragment was precipitated with 3% trichloroacetic acid and passed through a 40 cm × 1 cm Sephadex G-25 column, equilibrated in 50 mM Tris-HCl (pH 7.5) and 150 mM KCl (buffer A). Typically, the contamination represents less than 2% of the total binding capacity. Ca^{2+} and Mg^{2+} concentrations were determined with a Perkin-Elmer 2380 atomic absorption spectrophotometer.

Flow dialysis on 40 μM HsCen3 was carried out in the absence or presence of 0.05, 0.1, 0.2, 0.5, 1.0, 2, and 5 mM Mg^{2+} at 25 °C in buffer A according to the modified method of Colowick and Womack (*28*). Treatment of the raw data and evaluation of the binding parameters were carried out as previously described (*29*). The data were analyzed with the Adair equation for three binding sites:

$$\nu = (K_1[Ca^{2+}] + 2K_1K_2[Ca^{2+}]^2 + 3K_1K_2K_3[Ca^{2+}]^3)/(1 + K_1[Ca^{2+}] + K_1K_2[Ca^{2+}]^2 + K_1K_2K_3[Ca^{2+}]^3)$$

where K_1-K_3 are the stoichiometric association constants for the binding of the first, second, and third Ca^{2+} to the protein, respectively. The intrinsic association constants used in this study to present the data are linked to the stoichiometric ones by statistical factors of 3, 1, and $^1/_3$, respectively. After each experiment, SDS−PAGE was carried out on the protein solution to assess protein integrity.

Direct Mg^{2+} binding was studied by equilibrium gel filtration at room temperature as reviewed previously (*29*) in buffer A containing 50 μM EGTA to complex contaminating Ca^{2+}. The antagonism between Ca^{2+} and Mg^{2+} was tested with the competition equation for each site. $K'_{Ca}/K'_{Ca.app} = 1 + K'_{Mg.comp}[Mg^{2+}]$, where K'_{Ca} and $K'_{Ca.app}$ are the intrinsic Ca^{2+} binding constants for a given site in the absence and presence of Mg^{2+}, respectively, and $K'_{Mg.comp}$ is the calculated Mg^{2+} binding constant for this site.

Interaction with Hydrophobic Probes. The Ca^{2+}-dependent changes in the hydrophobic exposed surface of HsCen3 and its 11 kDa fragment were followed by monitoring the fluorescence properties of TNS as described previously (*30*). The Ca^{2+} and Mg^{2+} titrations were carried out on 2 μM metal-free protein in buffer A. The Ca^{2+} titration was also carried out in the presence of 2 mM Mg^{2+}, to start with the Mg^{2+} form instead of the apo form.

Interaction with Melittin. The interaction of HsCen3 and the 11 kDa fragment with ME was monitored by nondenaturing PAGE as previously described for CaM (*31*) and by covalent cross-linking followed by SDS−PAGE (*30*). Complex formation was also characterized by Trp fluorimetry as described for HsCen2 (*18*).

CD Spectroscopy. CD experiments were performed on a Jasco 715 CD spectrometer equipped with a Peltier temperature control unit. Far-UV spectra were recorded between 200 and 250 nm at 20 °C using 1 mm quartz cells. Spectra were collected as an average of four scans, with a scan speed of 20 nm/min and a response time of 2 s. Samples were dissolved in 14 mM MOPS buffer (pH 7.4) containing 24 mM NaCl. Temperature denaturation curves were recorded between 20 and 95 °C with a rate of temperature increase of 1 °C/min.

Isothermal Titration Calorimetry. Thermodynamic parameters of molecular interactions between HsCen3 and target peptides at 30 °C were investigated by ITC using a MicroCal MCS instrument (MicroCal Inc., Northampton, MA). The proteins and peptides were equilibrated in the same buffer containing 50 mM MOPS (pH 7.4), 100 mM NaCl, and Ca^{2+} (1 mM) or EDTA (1 mM). In a standard experiment, the protein (10−20 μM) in the 1.337 mL calorimeter cell was titrated by the peptide (generally 10 times more concentrated) by ~30 successive automatic injections of 7−10 μL each. The first injection of 2 μL was ignored in the final data analysis. Integration of the peaks corresponding to each injection and correction for the baseline were carried out using Origin-based software provided by the manufacturer. Fitting of the data to various interaction models results in the stoichiometry (n), equilibrium binding constant (K_a), and enthalpy of complex formation (ΔH). The reported thermodynamic parameters represent an average of at least two experiments. Usually, control experiments, consisting of injecting peptide solutions into the buffer, were performed to evaluate the heat of dilution.

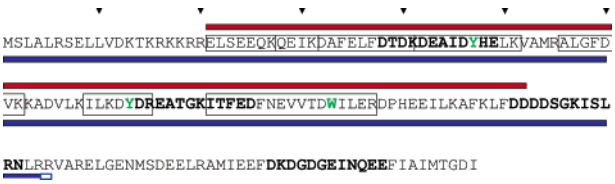

FIGURE 1: Amino acid sequence of HsCen3. The four EF-hand motifs are in bold. The trypsin peptides of the 11 kDa fragment identified by MALDI-TOF mass spectrometry are boxed. The red overlined polypeptide segment (10 899.1 Da) corresponds best to the experimentally determined molecular mass (10 900.5 Da) of the 11 kDa spontaneous fragment. The blue underlined polypeptide segment (14 821 and 14 665 Da) corresponds best to the experimentally determined molecular mass (14 823.1 and 14 660.0 Da, respectively) of the 14 kDa tryptic fragment. The near-UV-absorbing residues are highlighted in green.

RESULTS

Purification and Identification of the Spontaneous Cleavage Product of Hscen3. The metal-free form of HsCen3 is prone to spontaneous proteolysis, resulting in the appearance of a protein band of 11 kDa in SDS−PAGE. The action of the unidentified protease becomes evident after storage for 10 days at 4 °C and progresses after another 10 days. Mixtures of whole HsCen3 and the 11 kDa fragment could be separated by DE52 cellulose chromatography with a linear gradient from 0 to 200 mM KCl: the 11 kDa fragment elutes as a twin peak at 95 mM KCl. Alternatively, a protocol for fast separation was elaborated by Ca^{2+}-dependent phenyl Sepharose chromatography: the 11 kDa fragment was not retained, whereas the whole protein was retained in the presence of 1 mM Ca^{2+}. The latter was eluted with 1 mM EGTA. Mass spectrometric analysis yielded a molecular mass of 10 900.4 Da, and trypsin digestion followed by mass spectrometric analysis allowed identification of seven peptides of 10, all located between Glu 21 and Arg 97 (Figure 1). Therefore, there is strong evidence that the 11 kDa fragment corresponds to residues 21−112, and may be considered as the functional N-terminal half of HsCen3. In this study, this fragment is termed the 11 kDa endogenous fragment. The UV absorption spectra of the fragment and of whole HsCen3 are indistinguishable, as both contain three near-UV light absorption residues (Figure 1).

Limited Trypsin Proteolysis of HsCen3, Purification, and Identification of N-Terminal Polypeptides. Tryptic digestion (protease/HsCen3 ratio of 1/100) was carried out at 25 °C in 50 mM Tris-HCl (pH 7.5) and 1 mM Ca^{2+}. After 8 min, the digestion was stopped by addition of soybean trypsin inhibitor and 5% TCA precipitation. The peptides were separated by Sephadex G-50 gel filtration in 50 mM Tris-HCl (pH 7.5) and 50 mM Ca^{2+} and by DE52 cellulose chromatography as described above. Mass spectrometric analysis yielded twin peaks with molecular masses of 14 823.1 and 14 660.0 Da, suggesting that is comprises residues 1−124 and 1−125, respectively (Figure 1). Their UV spectra are identical to that of the whole HsCen3. In this study, this fragment is termed the 14 kDa fragment.

Direct Cation Binding Studies. Flow dialysis on apo-HsCen3 in the absence of Mg^{2+} yielded a biphasic isotherm (Figure 2) with one site of high affinity (K_d = 3.3 μM, no cooperativity) and two sites of low affinity (K_d = 140 μM, no cooperativity). The effect of Mg^{2+} on Ca^{2+} binding is antagonistic, but rather complex: with an increase in the

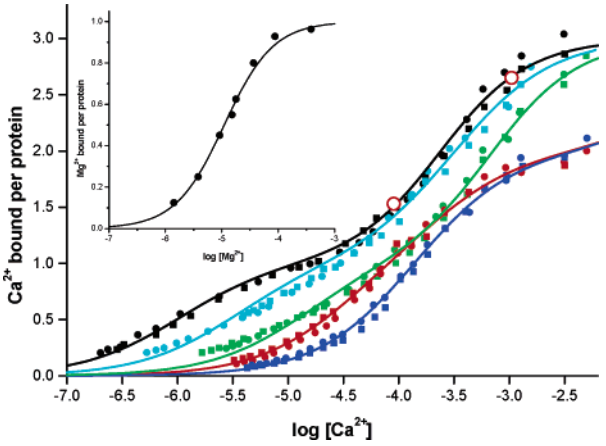

FIGURE 2: Binding of Ca^{2+} and Mg^{2+} to HsCen3. Direct Ca^{2+} binding to recombinant HsCen3 was monitored by flow dialysis at 25 °C in 50 mM Tris-HCl (pH 7.5) and 150 mM KCl (buffer A). The protein concentration is 25 μM. Duplicate (circles or squares) experiments are shown in the absence (black) or presence (filled symbols) of 0.05 (cyan), 0.1 (green), 0.5 (red), and 5 mM Mg^{2+} (blue). The solid lines are the theoretical isotherms calculated with the Adair equation for three sites with the intrinsic constants listed in Table 1. The large empty red circles represent the results of equilibrium gel filtration experiments in the presence of 90 μM and 1 mM Ca^{2+}, respectively (no Mg^{2+}). The inset shows direct binding of Mg^{2+} to HsCen3 monitored by equilibrium gel filtration in buffer A containing 50 μM EGTA.

Table 1: Intrinsic Ca^{2+} Binding Constants of HsCen3 at Different Mg^{2+} Concentrations Derived from the Stoichiometric Constants which Were Obtained by Fitting All of the Data to the Adair Equation for Three Sites

$[Mg^{2+}]$ (mM)	K'_1 (M^{-1})	K'_2 (M^{-1})	K'_3 (M^{-1})
0	3.3×10^5	7.0×10^3	7.5×10^3
0.05	1.1×10^5	6.5×10^3	4.5×10^3
0.1	2.6×10^4	2.4×10^3	2.6×10^3
0.2	1.7×10^4	3.0×10^3	1.0×10^2
0.5	1.3×10^4	4.0×10^3	6.0×10
1.0	1.0×10^4	3.0×10^3	6.0×10
2.0	6.2×10^3	3.0×10^3	6.0×10
5.0	5.0×10^3	1.2×10^3	6.0×10

concentration of free Mg^{2+} from 0 to 0.1 mM, the single high-affinity site rapidly loses its affinity for Ca^{2+}, so above 0.1 mM Mg^{2+} this site does not bind Ca^{2+} anymore under the conditions of flow dialysis. Presumably, above 0.2 mM, the bound Mg^{2+} does not dissociate from the high-affinity site. The two sites of low affinity for Ca^{2+} are much less affected by an increase in the Mg^{2+} concentration. Table 1 shows the intrinsic association constants K'_n extracted from the analysis of the ensemble of binding data. Assuming a direct competition between Ca^{2+} and Mg^{2+}, the calculated K_d for Mg^{2+} amounts to 10 μM, in excellent agreement with the direct Mg^{2+} binding experiment (see below). These observations suggest that the high-affinity site is of mixed Ca^{2+}/Mg^{2+} type.

When binding of Mg^{2+} to HsCen3 was assayed with equilibrium gel filtration in buffer A containing 50 μM EGTA, an isotherm without any cooperativity was obtained with a K_d value of 11 μM and a stoichiometry of 0.98 (Figure 2, inset). These data suggest that HsCen3 contains one Ca^{2+}/Mg^{2+} mixed site with a high affinity for both Ca^{2+} and Mg^{2+}, and two low-affinity Ca^{2+} binding sites, comparable to those measured for several S100 proteins (*32*). Despite their selectivity, the Ca^{2+} affinity of these latter sites is influenced by Mg^{2+}, probably by an allosteric interaction.

The ion binding to the 11 kDa tryptic fragment was monitored by equilibrium gel filtration: 0.97 and 1.6 Ca^{2+} ions bound at 51 and 875 μM free Ca^{2+}, respectively, whereas 0.89 Mg^{2+} ion is bound at 95 μM free Mg^{2+} in EGTA-containing buffer A. These data suggest that the fragment contains the high-affinity Ca^{2+}/Mg^{2+} mixed site and one of the low-affinity Ca^{2+}-specific site.

Ion Binding Assessed by ITC. We also explored the ion binding properties of HsCen3 by using isothermal titration calorimetry (ITC). Under our experimental conditions [20 μM HsCen3 and 350−500 μM $CaCl_2$ or $MgCl_2$ in 50 mM MOPS buffer (pH 7.4) and 100 mM NaCl], only the strong binding site is expected to be observed. The binding isotherm at 30 °C indeed shows a single binding event with a stoichiometry of 1:1, and dissociation constants of 8 and 28 μM were determined for Ca^{2+} and Mg^{2+}, respectively. These results confirm the capacity to bind strongly both Ca^{2+} and Mg^{2+} ions, as well as the relative affinity ratio between the two cations. The dissociation constants estimated by ITC are 2−3-fold larger than those measured by flow dialysis. Besides the difference in temperature and ionic conditions, it is likely that in the calorimetric experiments, the contribution of the weak binding sites (although too small to be confidently distinguished) could distort the binding isotherm, which was fitted to a simple one-site model. For both cations, binding to HsCen3 is exothermic ($\Delta H = -6.0$ and -7.4 kcal/mol for Ca^{2+} and Mg^{2+}, respectively) and enthalpy-driven.

Global Structural Characterization and Trp Fluorescence. CD spectroscopy is a practical and efficient method for a general structural characterization of a soluble protein. As shown in Figure 3A, the far-UV CD spectrum of the protein in the absence of Ca^{2+} shows two minima at 207 and 222 nm, which is typical for a protein with a significant α-helical secondary structure (*33*). A rough estimation, based on the linear relationship between the molar ellipticity at 222 nm and the helix content in α-helix/coil mixtures, suggests that 27% of the residues have α-helix-type backbone dihedral angles. This helical content is smaller than could be expected from a well-structured EF-hand protein, but similar to that observed under the same physical conditions with HsCen2 (*17*). Addition of Ca^{2+} induces a 32% increase in the overall CD intensity, accompanied by a change in the ratio between the negative bands at 222 and 207 nm from 0.81 to 0.89, most probably resulting from a Ca^{2+}-induced increase in the α-helix content and decrease in the conformational flexibility of the protein (see below). A similar spectral change (the peak ratio becomes 0.98) was observed when Mg^{2+} was added (Figure 3A). An additional increase in ellipticity (30% relative to the Ca^{2+} form) was noted when Ca^{2+}-saturated HsCen3 was mixed with an equimolar concentration of a target peptide (P1-XPC), while the 222 nm:207 nm peak ratio became slightly larger than 1. Note that the peptide alone, at the same concentration, gives a random coil-type spectrum, and that the ellipticity increase at 222 nm in the complex is larger that the sum of the contributions from the isolated molecules. The CD observations indicate that Ca^{2+}, Mg^{2+}, and target peptide binding induce important secondary and/or tertiary structure changes in HsCen3, similar to those noted for HsCen2 (*17*).

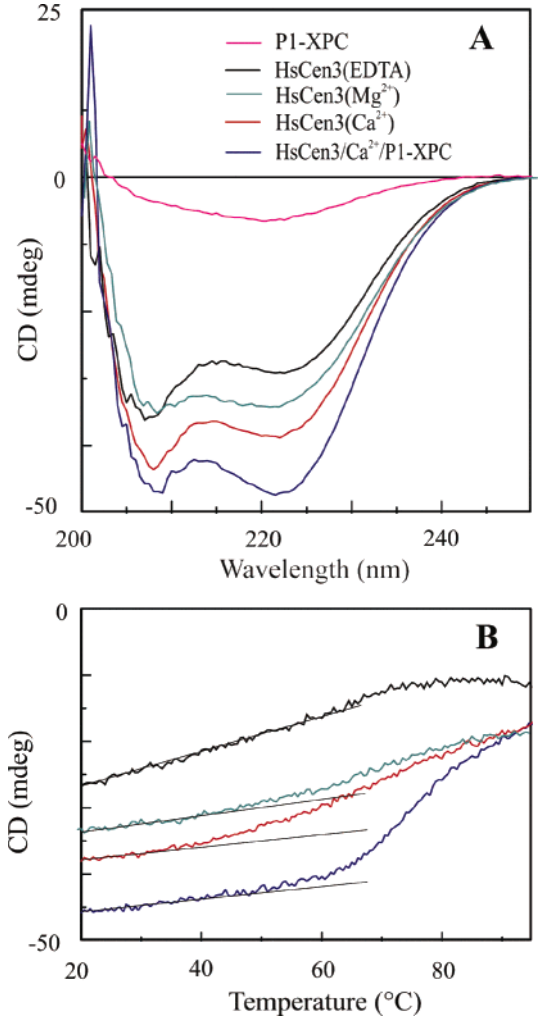

FIGURE 3: Circular dichroism analysis. (A) Far-UV spectra of 20 μM HsCen3 in 14 mM MOPS buffer (pH 7.4) and 24 mM NaCl in the presence of 1 mM $CaCl_2$ (red), 1 mM EDTA (black), 1 mM EGTA and 1 mM $MgCl_2$ (green), or 1 mM $CaCl_2$ and 20 μM P1-XPC (blue). Also shown is the spectrum of 20 μM P1-XPC in the same buffer (magenta). (B) Thermal denaturation curves, monitored by the CD band intensity at 222 nm. The samples are represented by the same colors as in panel A. The thin straight lines at the beginning of the records are only intended to underscore the initial baseline of the denaturation process.

The structural stability, as assessed by the thermal denaturation experiments, also exhibits a significant sensitivity to the interaction with dications or peptides (Figure 3B). The ellipticity at 222 nm in the apo form decreases steadily from 20 °C and reaches a plateau at ~70 °C. The absence of a clear cooperative transition reflects a loosely organized structure (*34*) that progressively unfolds fluctuating helical segments with a temperature increase. In the Ca^{2+}-saturated protein, the denaturation profile is different: a broad sigmoidal transition starts at 30 °C and shows a midtemperature at ~70 °C. A similar behavior was observed for the Mg^{2+} form. Addition of the peptide P1-XPC in the presence of Ca^{2+} further stabilizes the structure of HsCen3: the baseline is prolonged up to 50 °C and is followed by a cooperative unfolding centered around 80 °C. In contrast with HsCen2 (*17*), HsCen3 shows a single-step unfolding process in both the presence and absence of P1-XPC, suggesting a distinct structural relationship between the two EF-hand domains.

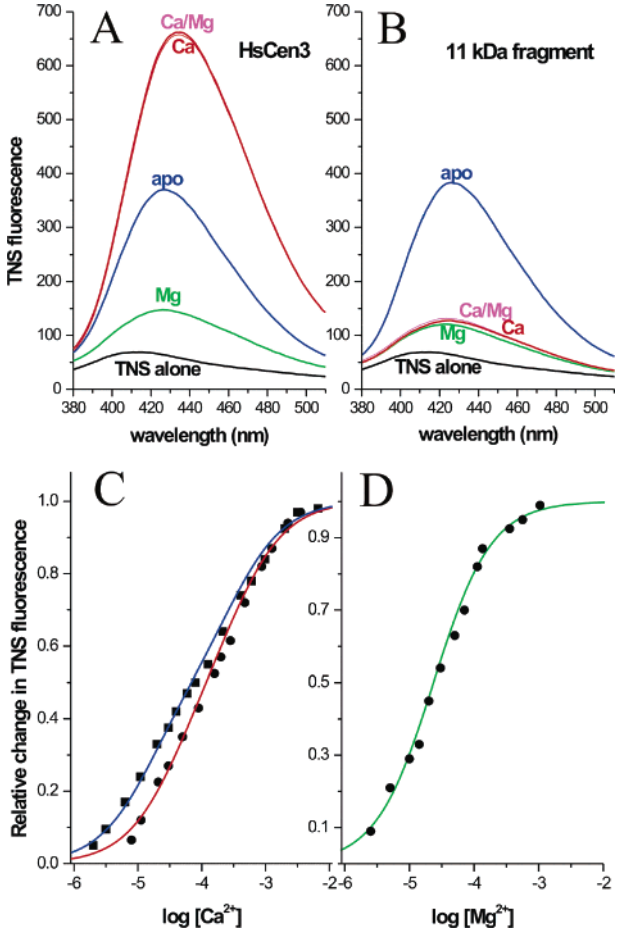

FIGURE 4: Ca^{2+}-dependent exposure of hydrophobic side chains. Hydrophobic exposure was monitored at 25 °C in 50 mM Tris-HCl (pH 7.5) and 150 mM KCl with the hydrophobic TNS. (A) Emission fluorescence spectra of TNS alone (black) and with whole HsCen3 in the presence of 50 μM EGTA (blue), 1 mM Mg^{2+} (green), 1 mM Ca^{2+} (red), or 1 mM $CaCl_2$ and $MgCl_2$ (magenta). (B) Same spectra for the 11 kDa endogenous fragment of HsCen3. (C) Ca^{2+} titrations of the TNS fluorescence change of HsCen3 in the absence (●) and presence of 1 mM Mg^{2+} (■). The fluorescence was measured at 438 nm and normalized to relative changes. The theoretical curves are calculated with the Adair equation for two sites with the following intrinsic constants: 2.8×10^4 and 6.4×10^3 M^{-1} without Mg^{2+} and 3.5×10^4 and 6.0×10^3 M^{-1} with 1 mM Mg^{2+}. (D) Mg^{2+} titration. The theoretical curve was calculated with the Adair equation for one site with an intrinsic constant of 4.0×10^4 M^{-1}.

The fluorescence spectra of the single Trp93, located in the linker segment between the two halves (Figure 1), suggest that in the native protein the Trp is well-protected from the solvent, since addition of 4 M guanidine-HCl leads to a red shift from 342 to 351 nm and a 2-fold decrease in the fluorescence intensity. The Trp fluorescence is weakly affected by the binding of dications (data not shown), with a 1.3-fold increase in the emission intensity upon binding of Ca^{2+}, and almost no change upon binding of Mg^{2+}. The 11 kDa endogenous fragment of HsCen3 behaved in a manner similar to that of whole HsCen3.

Interaction with Hydrophobic Probes. Metal-free HsCen3 enhances the fluorescence of the hydrophobic probe TNS 4-fold with a maximum at 426 nm (Figure 4A). When Ca^{2+} binds, the fluorescence emission further increases 2-fold and is red-shifted to 433 nm. In contrast, binding of Mg^{2+} leads to a 2-fold decrease in fluorescence as compared to that of

the apo form, and the resulting spectrum is close to that of TNS alone. These data, together with the thermal denaturation results, strongly suggest that the metal-free protein has a loosely folded conformation, close to the molten globule (MG) state. Additional support for the MG state is that limited trypsin proteolysis in 1 mM EGTA leads to very fast (within 10 min) and complete proteolysis, whereas in the presence of Ca^{2+} or Mg^{2+}, a 14 kDa band accumulates and remains stable with respect to proteolysis for more than 1 h (data not shown). The Ca^{2+}-induced fluorescence enhancement of TNS is likely due to the exposure of a large hydrophobic surface, since HsCen3 binds to phenyl-Sepharose in the presence of Ca^{2+} and is eluted upon replacement of Ca^{2+} by EGTA. The Mg^{2+}-induced decrease in fluorescence indicates that the protein changes from a MG state to a well-structured globular protein, but lacking exposed hydrophobic patches. In agreement with this observation, the Mg^{2+} form does not bind to phenyl-Sepharose.

The metal-free 11 kDa endogenous fragment of HsCen3 enhanced the TNS fluorescence to the same degree as the whole protein, and the binding of Mg^{2+} led to the same reduction in intensity (Figure 4B). However, contrary to the whole HsCen3, the addition of Ca^{2+} did not induce a fluorescence increase, but a decrease to the same extent as Mg^{2+} did. It thus seems clear that the N-terminal half of HsCen3 behaves like a structural unit which adopts the MG state in the ion-free state and a compact, ordered conformation upon binding of Ca^{2+} or Mg^{2+}. However, this domain is unable to form the exposed hydrophobic patch, which seems to be a specific property of the C-terminal half.

Titration of the TNS−apo-HsCen3 complex or the TNS−11 kDa fragment complex with Ca^{2+} or Mg^{2+} yields information about the affinity of the complex for the cations. The $[Ca^{2+}]_{0.5}$ value was 155 μM (Figure 4C), very similar to the K_d of the two low-affinity sites, meaning that binding of Ca^{2+} to the low-affinity sites is instrumental in the formation of the hydrophobic patch on the protein surface. In the presence of 2 mM Mg^{2+}, the $[Ca^{2+}]_{0.5}$ value was 60 μM, leading to the suggestion that binding of Ca^{2+} to the compact and ordered Mg^{2+} form is thermodynamically favored over binding of Ca^{2+} to a molten globule state. The $[Mg^{2+}]_{0.5}$ was 25 μM (Figure 4D), which is comparable to the value found by flow dialysis studies and very similar to the ITC results. Interestingly, for the TNS−11 kDa fragment complex, which can only proceed from the molten globule state to the ordered structure, the $[Ca^{2+}]_{0.5}$ and $[Mg^{2+}]_{0.5}$ values were 1.5 and 19 μM, respectively (data not shown), indicating that the binding of any of the two cations to the single high-affinity site is enough to induce the structural transition from the MG to the ordered state.

Interaction with Melittin. The presence of an exposed hydrophobic area in the Ca^{2+} form of HsCen3 was similarly observed in HsCen2 (*18*), which is able to bind melittin. It was thus tempting to examine also HsCen3 for the interaction with this target model. First, the interaction with ME was monitored by native PAGE on mixtures of 5 μg of HsCen3 and increasing amounts of ME (Figure 5A). The Ca^{2+}-, Mg^{2+}-, and metal-free forms of HsCen3 migrate with mobilities of 0.38, 0.46, and 0.62, respectively, whereas the positively charged ME alone does not enter the gel. At a 1:1 protein:peptide molar ratio, approximately half of the protein migrates as a complex with a well-defined mobility

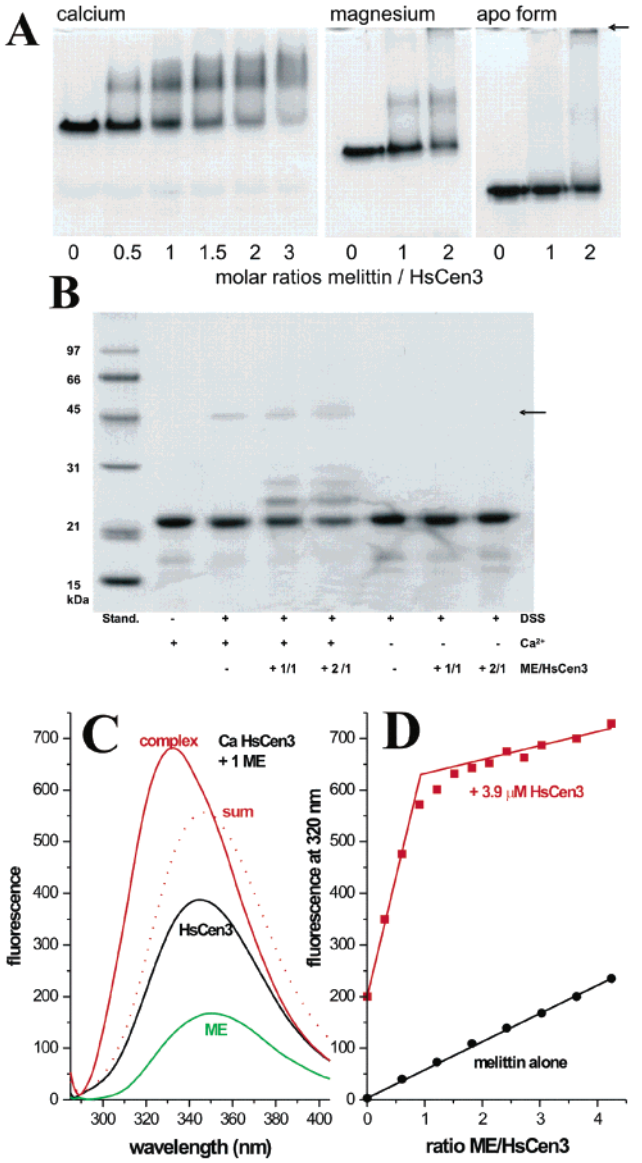

FIGURE 5: Interaction of melittin with HsCen3. (A) Native PAGE in the presence of 1 mM Ca^{2+}, Mg^{2+}, or EGTA. All lanes contained 0.3 nmol of HsCen3 and ME in increasing ratios as indicated. Free melittin does not migrate to the cathode in this native system. R_f values are 0.38 (Ca^{2+} form), 0.46 (Mg^{2+} form), and 0.83 (apo form) for HsCen3 and 0.26 for the 1:1 complex. (B) SDS−PAGE after covalent cross-linking. In the presence of DSS, HsCen3 exhibits a small amount of homodimer (arrow). When in addition ME is present, covalent conjugates containing 1:1 and 2:1 ME−HsCen3 complexes are seen. (C) Complex formation monitored by Trp fluorescence. The maximal intensity of the spectrum (solid red line) of the 1:1 complex is 1.23-fold higher that that of the theoretical sum (dotted red line) of the HsCen3 and ME spectra and is blue shifted by 16 nm. (D) Fluorescence titration of HsCen3 with ME in buffer A containing 1 mM $CaCl_2$.

of 0.26; at a 1:2 molar ratio, most of the free HsCen3 disappeared and the complex migrates as a smear with mobility ranging from 0.17 to 0.26. This suggests that with an increase in peptide concentration, first a well-defined 1:1 complex is formed, and later one or more MEs bind to the complex, thus forming a smear. No such complex was formed in the presence of EGTA, although aggregates are formed which do not enter the gel (arrow). Interestingly, in 1 mM Mg^{2+} and EGTA, a small amount of complex is formed, with a mobility of 0.31. The Mg^{2+}-induced complex

must involve the N-terminal domain, whereas the Ca^{2+}-induced complex involves the C-terminal domain and its hydrophobic patch.

We also examined the ME interaction with HsCen3 using the divalent cross-linker disuccinimidyl suberate (DSS) and SDS−PAGE (Figure 5B). HsCen3 alone treated with DSS exhibited a main band at 22 kDa, but also a faint band of 45 kDa, indicating that, like HsCen2 (*18*), the protein is partly homodimeric. This dimer band was not observed in the absence of Ca^{2+}. In the presence of ME, two major protein bands appear, one at 26 kDa corresponding to the 1:1 ME−centrin covalent adduct and one at 29 kDa corresponding to the 2:1 ME−HsCen3 complex.

Formation of a complex between HsCen3 and ME was also demonstrated by monitoring changes in the Trp fluorescence. Figure 5C shows that in the presence of Ca^{2+} the fluorescence spectrum of an equimolar mixture of HsCen3 and ME has a higher intensity and is more blue-shifted (from 348 to 332 nm) than the sum of spectra of the individual components. Only small changes occurred upon addition of a second ME, suggesting that, contrary to the first ME, binding of the second ME does not lead to major spectral perturbations (Figure 5D). Titration of HsCen3 with ME, monitored by the Trp fluorescence change at 320 nm, shows an inflection point at 0.91 ME/HsCen3; above this point, the fluorescence increases much less and can be attributed to the ME increments. The data points close to the inflection point allow estimation of a dissociation constant K_d of 20−50 nM, i.e., a 2−3-fold higher affinity than that of HsCen2 for ME.

Interaction with Target Peptides. ME is a useful model for the interaction of targets with members of the CaM superfamily, but more relevant biological information can be gathered with peptides that are known to represent centrin binding segments in Kar1p (*35*) or XPC (*25*). Therefore, we titrated HsCen3, in the presence or absence of Ca^{2+}, with these two peptides using the ITC technique. As illustrated in the thermogram of Figure 6A, P1-XPC forms a 1:1 complex with Ca^{2+}-saturated HsCen3 in an exothermic reaction (negative enthalpy). Fitting of the integrated data to a one-site binding model results in a high affinity (K_d = 13 nM) and a large binding enthalpy (−14.9 kcal/mol). As shown above, complex formation results in more helical content, and an increased thermal stability, suggesting that the peptide and/or additional fragments of the protein become more structured. The interaction parameters are comparable to those of HsCen2, although the binding free energy is lower, essentially due to a decreased enthalpy contribution (Table 2). During the binding experiments, we also noted, as in the case of HsCen2 (*17*), that the affinity of HsCen3 for the target decreases by almost 1 order of magnitude when NaCl is replaced by the same concentration of KCl. In the absence of Ca^{2+}, P1-XPC still binds to HsCen3, but because of an unfavorable entropy contribution, the affinity is 70-fold lower.

Similar experiments (Figure 6B) showed that P-Kar1p, the target peptide usually assayed for binding to various centrins (*22*), binds to Ca^{2+}-saturated HsCen3 (as well as to HsCen2), but with a significantly lower affinity (200 nM) and a lower enthalpy (−11.1 kcal/mol). Again, the metal-free form of HsCen3 interacts with this peptide with a reduced affinity (17-fold). For the two peptides, the binding entropy change

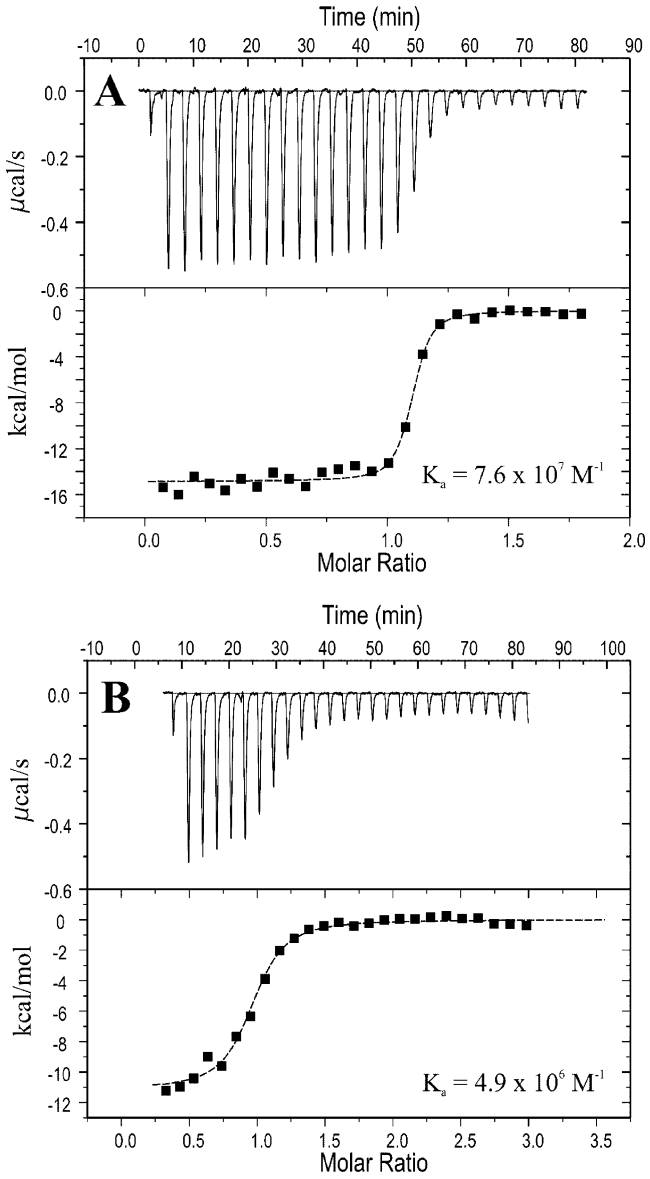

FIGURE 6: Target peptide binding. Titration of HsCen3 with (A) P1-XPC and (B) P-Kar1p peptides using ITC at 30 °C. Protein (10 μM) was dissolved in MOPS buffer (pH 7.4), 100 mM NaCl, and 1 mM $CaCl_2$, and the titrant was at a concentration of 100 μM in the same buffer.

is more negative when the protein is in the apo form since it includes a larger unfavorable contribution due to the transition from a fluctuating structural state to a more stable and persistent conformation.

DISCUSSION

Diversity in Ca^{2+} Binding. A characteristic feature of the proteins from the EF-hand superfamily is the wide diversity in the cation binding properties, including the affinity, kinetics, specificity, and cooperativity. CaM (*36*), vertebrate TnC (*37*), calcineurin B (*38*), and CLSP (*30*) all have four functional EF-hands, one pair in each domain of the protein. The two halves constitute more or less independent structural units. CaVP, which belongs to the CaM superfamily, has only one functional two-Ca^{2+}-binding pair in the C-terminal half (*39*). Except for the C-terminal pair in TnC and the N-terminal pair in CLSP, all these sites are quite specific for Ca^{2+}, i.e., interact poorly or not with Mg^{2+}, and have a

Table 2: Thermodynamic Parameters of the Interaction between HsCen2, HsCen3, and Target Peptides

protein	ligand	1 mM Ca^{2+}	K_d (error) (nM)	ΔH (error) (kcal/mol)	ΔG (kcal/mol)	$T\Delta S$
HsCen2[a]	P1-XPC	with	4.5 (0.8)	−27.2 (0.2)	−11.6	−15.6
HsCen2[a]	P1-XPC	without	125 (16)	−35.8 (0.6)	−9.6	−26.2
HsCen3	P1-XPC	with	13 (3)	−14.9 (0.4)	−10.9	−4.0
HsCen3	P1-XPC	without	909 (16)	−31 (1)	−8.4	−22.6
HsCen2	P-Kar1p	with	260 (34)	−13.3 (0.2)	−9.2	−4.1
HsCen3	P-Kar1p	with	200 (16)	−11.1 (0.4)	−9.3	−1.8
HsCen3	P-Kar1p	without	3300 (440)	−12 (0.7)	−7.6	−4.4

[a] From ref *17*.

moderate affinity (K_d = 1−10 μM under physiological conditions). They have been designated as activator or sensor sites (*40*). The centrins also belong to the CaM superfamily, but display great variance in their divalent cation binding properties. *Chlamydomonas* centrin may be more ancestral, since it kept four functional EF-hands in two distinct protein domains (*20*); one of the C-terminal sites has a very low affinity. HsCen2 evolved still farther away from the prototypical CaM and binds only one Ca^{2+} per monomer with a moderate affinity (K_d = 30 μM), but strict Ca^{2+} specificity (*18*). A particular truncated form of HsCen2, including the C-terminal half and helix D, can bind two Ca^{2+} ions per monomer (*19*), as does also the entire protein in a complex with melittin (*18*). In this study, we show that the closely related (sequence that is 53% identical) HsCen3 displays one high-affinity Ca^{2+}/Mg^{2+} mixed site and two low-affinity (K_d = 140 μM) Ca^{2+}-specific sites. The affinity of HsCen3 for Mg^{2+} is among the highest registered for EF-hand Ca^{2+}-binding proteins. At rest, Mg^{2+} occupies the high-affinity site and likely does not exchange for Ca^{2+} in moderately stimulated cells ($[Ca^{2+}]_{free} \leq 5-10$ μM). This suggests that the N-terminal domain of HsCen3 plays a structural rather than a regulatory role in the Ca^{2+} signaling processes.

As for the topology of the functional EF-hands in human centrins, we previously reported that HsCen2 binds its single Ca^{2+} to EF-hand IV in the C-terminal half (*19*). In MmCen4, the sequence of which is 74% identical to that of HsCen2, also only EF-hand IV seems to bind Ca^{2+} (*9*). Analysis of the HsCen3 sequence predicts (Table 3) that EF-hand III is inactive, mainly due to the N for E substitution in position 12 of the loop. We also note that EF-hand I is characterized by an unusual Glu in position 6 (between +*Z* and −*Y*), and EF-hand II should have a low affinity due to a Thr in position +*Z*. Our studies on the 11 kDa endogenous fragment and the 14 kDa tryptic fragment strongly suggest that the Ca^{2+}/Mg^{2+} binding site is situated in the N-terminal half, and it is tempting to attribute this site to EF-hand I, partly because it contains a *Z* acid pair (*41*−*43*). It should be noted that two other members of the CaM superfamily possess high-affinity Ca^{2+}/Mg^{2+} mixed sites: TnC in the two C-terminal EF-hands (*37*) and CLSP in the two N-terminal EF-hands (*18*). In TnC, the role of the C-terminal half is to bind TnC to the troponin complex in a Ca^{2+}/Mg^{2+}-dependent manner (*44*).

Metal-Induced Structural Changes. Cation binding to the single Ca^{2+}/Mg^{2+} mixed site seems to control an important structural transition from a molten globule state to a compact globular conformation. Indeed, the low α-helical content (27%), the absence of well-defined transitions in the CD melting curve, the strong interaction of apo-HsCen3 with TNS, and the high susceptibility of apo HsCen3 to proteolysis strongly suggest a loose packing. This structure can be described as a core of collapsed hydrophobic residues surrounded by α-helical segments which are in a dynamic equilibrium between various conformations over the entire peptide backbone. In HsCen3, the transition from the MG to the compact state clearly occurs when the high-affinity site is occupied by either Ca^{2+} or Mg^{2+}. The MG state also prevails in the metal-free state of various EF-hand proteins, including *Nereis* SCP (*45*, *46*) and calexcitin (*47*). HsCen3, NSCP, and calexcitin possess at least one high-affinity Ca^{2+}/Mg^{2+} mixed site, and in all three proteins, the transition is also controlled by interaction with either Ca^{2+} or Mg^{2+}. Under physiological conditions, the Ca^{2+}/Mg^{2+} site is always occupied by a divalent cation, and the protein is protected from the MG state, even at rest. It is plausible that the function of this site is to prevent the protein from adopting a MG state and being readily catabolized (*47*). Interestingly, a re-examination of our data on HsCen2 (see Figure 2 of ref *18* and Figure 4 of ref *19*), which does not interact with Mg^{2+}, incites us to propose that the C-terminal domain of metal-free HsCen2 also possesses a MG structure. Thus, in this protein, the transition from the MG to the native state is controlled by only Ca^{2+} binding to EF-hand IV. This is reminiscent of CaVP that also has only Ca^{2+}-specific sites, but behaves as a MG in the apo form (*39*, *48*). In conclusion, the MG state may be quite common in the apo forms of several EF-hand subfamilies. Proteins containing Ca^{2+} or Mg^{2+} can escape the MG state, and thus avoid degradation by the proteasome, since Mg^{2+} occupies the site under physiological resting conditions, whereas proteins with exclusively Ca^{2+}-specific sites may avoid the MG state by forming a permanent complex with a target peptide, as CaVP does (*49*).

One may question whether the whole apo-HsCen3 or only the N-terminal half adopts a MG state. Three experimental observations favor the first hypothesis. (1) The melting curve of the integral protein in Figure 3B shows no discrete structural transition. (2) Trypsin cleavage of native apo-HsCen3 results in very small fragments, much smaller than the size of the C-terminal half (data not shown). (3) The Ca^{2+} titration of the TNS fluorescence enhancement in the presence of whole HsCen3 shows no transition to the compact native state (weak TNS enhancement) before the solvent-exposed hydrophobic patch is formed (strong TNS enhancement). As suggested by the single transition in thermal denaturation, the two halves in HsCen3 are structurally much more interdependent than in HsCen2. The case of the N-terminal 11 kDa endogenous fragment is simpler,

Table 3: Ca^{2+}-Binding Loop Sequences in HsCen1−HsCen3, MmCen4, CrCen, and CaM[a]

		1 3 5 7 9 12
Site I	HsCen1	DVDGSGTIDAKE
	HsCen2	DADGTGTIDVKE
	HsCen3	DTDKDEAIDYHE
	MmCen4	DIDGSGTIDLKE
	CrCen	DTDGSGTIDAKE
	CaM	DKDGDGTITTKE
Site II	HsCen1	DREGTGKISFND
	HsCen2	DKEGTGKMNFGD
	HsCen3	DREATGKITFED
	MmCen4	DKEGTGTICFED
	CrCen	DKDGSGTIDFEE
	CaM	DADGNGTIDFPE
Site III	HsCen1	DDDETGKISFKN
	HsCen2	DDDETGKISFKN
	HsCen3	DDDDSGKISLRN
	MmCen4	DDDATGSISLNN
	CrCen	DDDNSGTITIKD
	CaM	DKDGNGYISAAE
Site IV	HsCen1	DRDGDGEVNEEE
	HsCen2	DRDGDGEVSEQE
	HsCen3	DKDGDGEINQEE
	MmCen4	DRDGDGEINEEE
	CrCen	DRNDDNEIDEDE
	CaM	DIDGDGQVNYEE

[a] In gray are residues with a lower occurrence in the corresponding position within the EF-hand family (*57*).

since Ca^{2+} binding can overcome the MG state and induces the compact globular state.

Like other members of the CaM superfamily, the Ca^{2+} form of HsCen3 exposes a hydrophobic patch on the surface that is monitored by TNS. TNS fluorescence enhancement results form binding either to the MG (see above) or to a solvent-exposed hydrophobic patch (*50*). The difference in maximal fluorescence wavelength, illustrated in Figure 4A, indicates that the two TNS binding sites have different natures. The hydrophobic exposure is confirmed by the fact that HsCen3 binds in a Ca^{2+}-dependent manner to phenyl-Sepharose. Mg^{2+} binding alone does not lead to hydrophobic exposure, as was also observed in CLSP (*30*). In fact, the hydrophobic exposure is concomitant with the binding of Ca^{2+} to low-affinity Ca^{2+}-specific site EF-hand IV in the C-terminal half of HsCen3. Interestingly, in the 11 kDa fragment, no hydrophobic patch could be induced, and it does not bind to phenyl-Sepharose. One may suppose that formation of the solvent-exposed hydrophobic patch is under the control of binding of Ca^{2+} to EF-hand IV, in both HsCen2 (*18*) and HsCen3 (this study).

Target Binding. Exposure of the hydrophobic patch is instrumental for the interaction with target proteins. As demonstrated for HsCen2 (*18*), ME is a good model for the study of intermolecular interactions. It also interacts with HsCen3, as we showed here by band shift in native PAGE, covalent cross-linking, and Trp fluorescence changes. However, the stoichiometry of the complex is two ME molecules per HsCen3 instead of one ME per HsCen2. In the CaM−ME complex, the N-terminal end of the ME α-helix interacts with the N-terminal half of the protein and the C-terminal end of ME with the C-terminal half of CaM (*51*). On the basis of the spectral similarities in the CaM−ME, HsCen2−ME, and HsCen3−ME complexes, we assume that HsCen3, through its C-terminal hydrophobic patch, interacts in a similar way with ME. In HsCen3, one more ME interacts with the N-terminal domain, provided Ca^{2+} or Mg^{2+} is bound, i.e., when this domain is not in the MG state. The latter interaction may be weaker and different in nature, since no hydrophobic surface is formed. CrCen (sequence that is 51% identical with that of HsCen3) also shows two distinct binding events, apparently related to the binding of one Kar1p peptide at each of the two halves (*20*).

The binding of ME places HsCen3 in the category of Ca^{2+} sensors, but more relevant information is gained by investigating the complex formation with peptides derived from physiological target proteins. Genetic and biochemical experiments allowed identification of several protein targets, including Kar1p (*21*), mps3p (*23*), and Sfi1 (*24*) in the centrosome/SPB, G-protein transducin in the connecting cilium of photoreceptor cells (*52*, *53*), and XPC (*25*) and Sac3 (*26*) in the nucleus region. Further, the binding peptides of Kar1p (*22*) and XPC (*17*) have been identified. The Ca^{2+} sensitivity of these interactions appears to be quite variable: while interaction with G-transducin, Kar1p, and XPC is more or less dependent on Ca^{2+} concentration, binding of Cdc31p to Sfi1 takes place even at 5 mM EGTA.

The reported variability of target interactions with centrins (*9*, *53*) incited us to test the potential for binding to HsCen3. In the presence of Ca^{2+}, both formed a complex, but with highly distinct affinities: $K_d = 13$ and 200 nM for P1-XPC and Kar1p, respectively. In the absence of Ca^{2+}, the HsCen3−P1-XPC complex exhibited a 70-fold lower affinity. As in the case of HsCen2, the binding processes are driven by favorable enthalpy changes and counteracted by negative entropy changes; i.e., the number of hydrophobic and electrostatic bonds largely compensates for the increase in the level of conformational order, especially in the target peptide (as evidenced by the gain in α-helix content). It should be noticed that in the majority of the CaM complexes with natural targets the driving force is also enthalpic (*54*−

56). Despite the promiscuity of molecular interactions in the CaM superfamily, we expect that details in the structure of the targets ensure the specificity of interactions. A specific feature of centrins is an extension of ~20 residues at the N-terminal end. In the case of HsCen3, this region includes an unusual basic sequence (KTKRKKRR) whose role may be related to the capacity of centrins to bind amphiphilic helices containing acidic residues.

Conclusion. Our study is a first step toward understanding the mode of action and functional diversity of centrins. Sequence comparison, and a number of functional properties, including Ca^{2+} binding affinities, Ca^{2+}/Mg^{2+} selectivity, and Ca^{2+} sensitivity of target binding, support the hypothesis that HsCen3, on one side, and HsCen1 or HsCen2, on the other side, belong to different functional classes. In their evolution toward more specificity in the target binding, they may have been driven into structures that are thermodynamically or biochemically unfavorable inside the cell. Therefore, the natural selection may have introduced restricted mutations to prevent the MG state. In the centrin field, two strategies seem to operate: introduction of a Ca^{2+}/Mg^{2+} mixed site (as in TnC) or a decrease in the Ca^{2+} dependency, to remain bound to the target protein under all cellular conditions.

ACKNOWLEDGMENT

We thank Damarys Loew and Lucas Signor for the help with mass spectrometry analysis.

REFERENCES

1. Bornens, M. (2002) Centrosome composition and microtubule anchoring mechanisms, *Curr. Opin. Cell Biol. 14*, 25−34.
2. Pihan, G. A., Purohit, A., Wallace, J., Malhotra, R., Liotta, L., and Doxsey, S. J. (2001) Centrosome defects can account for cellular and genetic changes that characterize prostate cancer progression, *Cancer Res. 61*, 2212−2219.
3. Brinkley, B. R. (2001) Managing the centrosome numbers game: From chaos to stability in cancer cell division, *Trends Cell Biol. 11*, 18−21.
4. Lingle, W. L., Barrett, S. L., Negron, V. C., D'Assoro, A. B., Boeneman, K., Wanguo, L., Whitehead, C. M., Reynolds, C., and Salisbury, J. L. (2002) Centrosome amplification drives chromosomal instability in breast tumor development, *Proc. Natl. Acad. Sci. U.S.A. 99*, 1978−1983.
5. Means, A. R. (1994) Calcium, calmodulin and cell cycle regulation, *FEBS Lett. 347*, 1−4.
6. Marshall, W. F., Vucica, Y., and Rosenbaum, J. L. (2001) Kinetics and regulation of de novo centriole assembly: Implications for the mechanism of centriole duplication, *Curr. Biol. 11*, 308−317.
7. Salisbury, J. L., Suino, K. M., Busby, R., and Springett, M. (2002) Centrin-2 is required for centriole duplication in mammalian cells, *Curr. Biol. 12*, 1287−1292.
8. Paoletti, A., Bordes, N., Haddad, R., Schwartz, C. L., Chang, F., and Bornens, M. (2003) Fission yeast cdc31p is a component of the half-bridge and controls SPB duplication, *Mol. Biol. Cell 14*, 2793−2808.
9. Gavet, O., Alvarez, C., Gaspar, P., and Bornens, M. (2003) Centrin4p, a novel mammalian centrin specifically expressed in ciliated cells, *Mol. Biol. Cell 14*, 1818−1834.
10. Wolfrum, U., Giessl, A., and Pulvermüller, A. (2002) Centrins, a novel group of Ca^{2+}-binding proteins in vertebrate photoreceptor cells, in *Photoreceptors and Calcium* (Baehr, W., and Palczewski, K., Eds.) pp 154−178, Kluwer Academic/Plenum Publishers, New York.
11. Hart, P. E., Glantz, J. N., Orth, J. D., Poynter, G. M., and Salisburry, J. L. (1999) Testis-specific murine centrin, Cetn1: Genomic characterization and evidence for retroposition of a gene encoding a centrosome protein, *Genomics 60*, 111−120.
12. Paoletti, A., Moudjou, M., Paintrand, M., Salisbury, J. L., and Bornens, M. (1996) Most of centrin in animal cells is not centrosome-associated and centrosomal centrin is confined to the distal lumen of centrioles, *J. Cell Sci. 109*, 3089−3102.
13. Spang, A., Courtney, I., Grein, K., Matzner, M., and Schiebel, E. (1995) The Cdc31p-binding protein Kar1p is a component of the half bridge of the yeast spindle pole body, *J. Cell Biol. 128*, 863−877.
14. Koblenz, B., Schoppmeier, J., Grunow, A., and Lechtreck, K.-F. (2003) Centrin deficiency in *Chlamidomonas* causes defects in basal body replication, segregation and maturation, *J. Cell Sci. 116*, 2635−2646.
15. Salisbury, J. L., Baron, A., Surek, B., and Melkonian, M. (1984) Striated flagellar roots: Isolation and partial characterization of a calcium-modulated contractile organelle, *J. Cell Biol. 99*, 962−970.
16. Sanders, M. A., and Salisbury, J. L. (1994) Centrin plays an essential role in microtubule severing during flagellar excision in *Chlamydomonas reinhardti*, *J. Cell Biol. 124*, 795−805.
17. Popescu, A., Miron, S., Blouquit, Y., Duchambon, P., and Craescu, C. T. (2003) *Xeroderma pigmentosum* group C protein possesses a high affinity binding site for human centrin 2 and calmodulin, *J. Biol. Chem. 278*, 40252−40261.
18. Durussel, I., Blouquit, Y., Middendorp, S., Craescu, C. T., and Cox, J. A. (2000) Cation- and peptide-binding properties of human centrin 2, *FEBS Lett. 472*, 208−212.
19. Matei, E., Miron, S., Blouquit, Y., Duchambon, P., Durussel, I., Cox, J. A., and Craescu, C. T. (2003) The C-terminal half of human centrin 2 behaves like a regulatory EF-hand domain, *Biochemistry 42*, 1439−1450.
20. Veeraraghavan, S., Fagan, P. A., Hu, H., Lee, V., Harper, J. F., Bessie, H., and Chazin, W. J. (2002) Structural independence of the two EF-hand domains of caltractin, *J. Biol. Chem. 277*, 28564−28571.
21. Baum, P., Furlong, C., and Byers, B. (1986) Yeast gene required for spindle pole body duplication: Homology of its product with Ca^{2+}-binding proteins, *Proc. Natl. Acad. Sci. U.S.A. 83*, 5512−5516.
22. Geier, B. M., Wiech, H., and Schiebel, E. (1996) Binding of centrins and yeast calmodulin to synthetic peptides corresponding to binding sites in the spindle pole body components Kar1p and Spc110p, *J. Biol. Chem. 271*, 28366−28374.
23. Jaspersen, S. L., Giddings, J. T. H., and Winey, M. (2002) Mps3p is a novel component of the yeast spindle pole body that interacts with the yeast centrin homologue Cdc31p, *J. Cell Biol. 159*, 945−956.
24. Kilmartin, J. V. (2003) Sfi1p has conserved centrin-binding sites and an essential function in budding yeast spindle body duplication, *J. Cell Biol. 162*, 1211−1221.
25. Araki, M., Masutani, C., Takemura, M., Uchida, A., Sugasawa, K., Kondoh, J., Ohkuma, Y., and Hanaoka, F. (2001) Centrosome protein centrin 2/caltractin 1 is part of the *Xeroderma pigmentosum* group C complex that initiates global genome nucleotide excision repair, *J. Biol. Chem. 276*, 18665−18672.
26. Fischer, T., Rodriguez-Navarro, Pereira, G., Racz, A., Schiebel, E., and Hurt, E. (2004) Yeast centrin Cdc31 is linked to the nuclear mRNA export machinery, *Nat. Cell Biol. 6*, 840−848.
27. Maulet, Y., and Cox, J. A. (1983) Structural changes in melittin and calmodulin upon complex formation and their modulation by calcium, *Biochemistry 22*, 5680−5686.
28. Colowick, S. P., and Womack, F. C. (1969) Binding of diffusible molecules by macromolecules: Rapid measurement by rate of dialysis, *J. Biol. Chem. 244*, 774−747.
29. Cox, J. A. (1996) in *Guidbook to the Calcium-Binding Proteins* (Celio, M. R., Pauls, T., and Schwaller, B., Eds.) pp 1−12, Oxford University Press, Oxford, U.K.
30. Durussel, I., Méhul, B., Bernard, D., Schmidt, R., and Cox, J. A. (2002) Cation- and peptide-binding properties of human calmodulin-like skin protein, *Biochemistry 41*, 5439−5448.
31. Comte, M., Maulet, Y., and Cox, J. A. (1983) Ca^{2+}-dependent high-affinity complex formation between calmodulin and melittin, *Biochem. J. 209*, 269−272.
32. Heizmann, C. W., and Cox, J. A. (1988) New perspectives on S100 proteins: A multi-functional Ca^{2+}-, Zn^{2+}- and Cu^{2+}-binding protein family, *BioMetals*, 383−397.
33. Johnson, W. C. (1999) Analysing protein circular dichroism spectra for accurate secondary structures, *Proteins: Struct., Funct., Genet. 35*, 307−312.
34. Tsalkova, T. N., and Privalov, P. L. (1985) Thermodynamic study of domain organization in troponin C and calmodulin, *J. Mol. Biol. 181*, 533−544.

35. Wiech, H., Geier, B. M., Paschke, T., Spang, A., Grein, K., Steinkötter, J., Melkonian, M., and Schiebel, E. (1996) Characterization of green alga, yeast, and human centrins, *J. Biol. Chem. 271*, 22453−22461.
36. Milos, M., Schaer, J. J., Comte, M., and Cox, J. A. (1986) Calcium-proton and calcium-magnesium antagonisms in calmodulin: Microcalorimetric and potentiometric analyses, *Biochemistry 25*, 6279−6287.
37. Potter, J. D., and Gergely, J. (1975) The calcium and magnesium binding sites on troponin and their role in the regulation of myofibrillar adenosine triphosphatase, *J. Biol. Chem. 250*, 4628−4633.
38. Feng, B., and Stemmer, P. M. (1999) Interactions of calcineurin A, calcineurin B, and Ca^{2+}, *Biochemistry 38*, 12481−12489.
39. Petrova, T. V., Comte, M., Takagi, T., and Cox, J. A. (1995) Thermodynamic and molecular properties of the interaction between amphioxus calcium vector protein and its 26 kDa target, *Biochemistry 34*, 312−318.
40. Crivici, A., and Ikura, M. (1995) Molecular and structural basis of target recognition by calmodulin, *Annu. Rev. Biophys. Biomol. Struct. 24*, 85−116.
41. Henzl, M. T., Hapak, R. C., and Goodpasture, E. A. (1996) Introduction of a fifth carboxylate ligand heightens the affinity of the oncomodulin CD and EF sites for Ca^{2+}, *Biochemistry 35*, 5856−5869.
42. Tikunova, S. B., Black, D. J., Johnson, J. D., and Davis, J. P. (2001) Modifying Mg^{2+} binding and exchange with the N-terminal of calmodulin, *Biochemistry 40*, 3348−3353.
43. Davis, J. P., Rall, J. A., Reiser, P. J., Smillie, L. B., and Tikunova, S. B. (2002) Engineering competitive magnesium binding into the first EF-hand of skeletal troponin C, *J. Biol. Chem. 277*, 49716−49726.
44. Cox, J. A., Comte, M., and Stein, E. A. (1981) Characterization of a new sarcoplasmic calcium-binding protein with magnesium-induced cooperativity in the binding of calcium, *Biochem. J. 195*, 205−311.
45. Prêcheur, B., Cox, J. A., Petrova, T., Mispelter, J., and Craescu, C. T. (1996) Nereis sarcoplasmic Ca^{2+}-binding protein has a highly unstructured apo state which is switched to the native state upon binding of the first Ca^{2+} ion, *FEBS Lett. 395*, 89−94.
46. Christova, P., Cox, J. A., and Craescu, C. T. (2000) Ion-induced conformational and stability changes in Nereis sarcoplasmic calcium binding protein: Evidence that the apo state is a molten globule, *Proteins: Struct., Funct., Genet. 40*, 177−184.
47. Gombos, Z., Durussel, I., Ikura, M., Rose, D. R., Cox, J. A., and Chakrabartty, A. (2003) Conformational coupling of Mg^{2+} and Ca^{2+} on the three-state folding of calexcitin B, *Biochemistry 42*, 5531−5539.
48. Théret, I., Baladi, S., Cox, J. A., Sakamoto, H., and Craescu, C. T. (2000) Sequential calcium binding to the regulatory domain of calcium vector protein reveals functional assymmetry and is accompanied by large structural changes, *Biochemistry 39*, 7920−7926.
49. Cox, J. A. (1986) Isolation and characterization of a new Mr 18,-000 protein with calcium vector properties in amphioxus muscle and identification of its endogenous target protein, *J. Biol. Chem. 261*, 13173−13178.
50. Tanaka, T., and Hidaka, H. (1980) Hydrophobic regions function in calmodulin-enzyme(s) interactions, *J. Biol. Chem. 255*, 11078−11080.
51. Scaloni, A., Miraglia, N., Orrù, S., Amodeo, P., Motta, A., Marino, G., and Pucci, P. (1998) Topology of the calmodulin-melittin complex, *J. Mol. Biol. 277*, 945−958.
52. Pulvermuller, A., Giessl, A., Heck, M., Wottrich, R., Schmitt, A., Ernst, O. P., Choe, H. W., Hofmann, K. P., and Wolfrum, U. (2002) Calcium-dependent assembly of centrin-G-protein complex in photoreceptor cells, *Mol. Cell. Biol. 22*, 2194−2203.
53. Giessl, A., Pulvermuller, A., Trojan, P., Park, J. H., Choe, H.-W., Ernst, O. P., Hofmann, K. P., and Wolfrum, U. (2004) Differential expression and interaction with the visual G-protein transducin of centrin isoforms in mammalian photoreceptor cells, *J. Biol. Chem. 279*, 51472−51481.
54. Milos, M., Schaer, J. J., Comte, M., and Cox, J. A. (1988) Microcalorimetric investigation of the interaction of calmodulin with seminalplasmin and myosin light chain kinase, *J. Biol. Chem. 263*, 9218−9222.
55. Wintrode, P. L., and Privalov, P. L. (1997) Energetics of target peptide recognition by calmodulin: A calorimetric study, *J. Mol. Biol. 266*, 1050−1062.
56. Brokx, R. D., Lopez, M. M., Vogel, H. J., and Makhatadze, G. I. (2001) Energetics of target peptide binding by calmodulin reveals different modes of binding, *J. Biol. Chem. 276*, 14083−14091.
57. Falke, J. J., Drake, S. K., Hazard, A. L., and Peersen, O. B. (1994) Energetics of target peptide binding by calmodulin reveals different modes of binding, *Q. Rev. Biophys. 27*, 219−290.

BI048294E